Non-local energy transfers in rotating turbulence at intermediate Rossby number

L. Bourouiba[1]†, D. N. Straub[2] and M. L. Waite[3]

[1] Department of Mathematics, Massachusetts Institute of Technology Cambridge, MA 02139-4307, USA

[2] Department of Atmospheric and Oceanic Sciences, McGill University, Montréal, QC H3A 2K6, Canada

[3] Department of Applied Mathematics, University of Waterloo, 200 University Avenue West, Waterloo, Ontario N2L 3G1, Canada

Turbulent flows subject to solid-body rotation are known to generate steep energy spectra and two-dimensional columnar vortices. The localness of the dominant energy transfers responsible for the accumulation of the energy in the two-dimensional columnar vortices of large horizontal scale remains undetermined. Here, we investigate the scale-locality of the energy transfers directly contributing to the growth of the two-dimensional columnar structures observed in the intermediate Rossby number (*Ro*) regime. Our approach is to investigate the dynamics of the waves and vortices separately: we ensure that the two-dimensional columnar structures are not directly forced so that the vortices can result only from association with wave to vortical energy transfers. Detailed energy transfers between waves and vortices are computed as a function of scale, allowing the direct tracking of the role and scales of the wave–vortex nonlinear interactions in the accumulation of energy in the large two-dimensional columnar structures. It is shown that the dominant energy transfers responsible for the generation of a steep two-dimensional spectrum involve direct non-local energy transfers from small-frequency small-horizontal-scale three-dimensional waves to large-horizontal-scale two-dimensional columnar vortices. Sensitivity of the results to changes in resolution and forcing scales is investigated and the non-locality of the dominant energy transfers leading to the emergence of the columnar vortices is shown to be robust. The interpretation of the scaling law observed in rotating flows in the intermediate-*Ro* regime is revisited in the light of this new finding of dominant non-locality.

Key words: homogeneous turbulence, rotating turbulence, wave–turbulence interactions

1. Introduction

The non-dimensional Rossby number is a key parameter in rotating flows. It is defined as $Ro = U/2\Omega L \sim \tau_\Omega/\tau_{nl}$, where U is the characteristic flow velocity, Ω the rotation rate, L the characteristic length scale of the flow, and τ_Ω and τ_{nl} are the rotation and nonlinear turnover time scales, respectively. *Ro* is the ratio of magnitudes of the nonlinear term to the Coriolis acceleration in the Navier–Stokes equations

† Email address for correspondence: lbouro@mit.edu

expressed in a rotating frame. Turbulent flows dominated by strong rotation have low Ro and show substantial departure from the classical phenomenology of isotropic three-dimensional turbulence. Such flows have been the subject of many studies due to their ubiquity in geophysical and astrophysical flows that can have Ro values of 0.1 or lower (e.g. Greenspan 1968; Pedlosky 1987).

In the $Ro = 0$ linear limit, the Taylor–Proudman theorem states that the slow dynamics (quasi-steady) is associated with the velocity field that is invariant in the direction of the background rotation, corresponding to two-dimensional slow modes, while the linear time-varying equations have inertial wave solutions with anisotropic dispersion equation $\omega_{s_k} = s_k 2\boldsymbol{\Omega} \cdot \boldsymbol{k}/|\boldsymbol{k}|$, where $s_k = \pm$, $\boldsymbol{k}$ is the wavenumber, and $\boldsymbol{\Omega}$ is the rotation vector chosen to be vertical herein ($\boldsymbol{\Omega} = \Omega\hat{z}$) (Greenspan 1968).

In the small- but non-zero-Ro regime which is relevant for geophysical flows, nonlinearity is restored, but the linear wave dynamics continues to play a significant role. Building on the linear results, we keep the linear mode decomposition when analysing properties of the flow. The zero-frequency $\omega_k = 0$ modes are the slow modes corresponding to the vertically averaged flow or columnar vortices, while the non-zero frequency modes correspond to inertial waves with $|\omega_{s_k}| < 2\Omega$. The former form a two-dimensional three-component field with horizontal vertically averaged (x, y) components (two-dimensional two-component field $\boldsymbol{u}_{2D}$) denoted two-dimensional or vortical; and a third vertical (z) vertically averaged component denoted w. The latter form a three-dimensional three-component field of inertial waves denoted $\boldsymbol{u}_{3D}$.

1.1. *Effects of rotation on turbulence: focus on two-dimensionalization*

Numerous laboratory studies examining turbulent flows dominated by rotation (small Ro) observed inertial wave propagation, anisotropy development, a reduction of the rate of energy dissipation, and the emergence of anisotropic large-scale columnar structures from initially isotropic turbulence leading to a general tendency of the flow to become two-dimensional as Ro decreases below one (e.g. Hide & Ibbertson 1966; Ibbetson & Tritton 1975; McEwan 1976; Hopfinger, Browand & Gagne 1982; Jacquin *et al.* 1990; Morize & Moisy 2006; Bewley *et al.* 2007; Staplehurst, Davidson & Dalziel 2008). Such experimental observations were complemented by works using the controlled setting of numerical simulations of forced and decaying rotating turbulent flows (e.g. Bardina, Ferziger & Rogallo 1985; Bartello, Métais & Lesieur 1994; Hossain 1994; Smith & Waleffe 1999; Chen *et al.* 2005; Bourouiba & Bartello 2007; Thiele & Müller 2009). In decaying turbulence, an intermediate regime has been identified between the weakly rotating and small-Rossby-number limits (Bourouiba & Bartello 2007). The intermediate-Ro regime is characterized by a maximum of nonlinear coupling between two-dimensional and three-dimensional modes as defined above. A distinct growth of two-dimensional columnar vortices and peak of asymmetry between cyclonic and anticyclonic columnar vortices is observed at $Ro \approx 0.2$. More recent numerical simulations of decaying turbulence also recovered the emergence of the columnar vortices in the intermediate-Ro regime and an anisotropy in the energy transfers observed to be damped in the direction of $\boldsymbol{\Omega}$ only (Thiele & Müller 2009).

Both nonlinear (e.g. Zhou 1995; Babin, Mahalov & Nicolaenko 1996; Cambon & Scott 1999) and linear (Staplehurst *et al.* 2008) effects were proposed to explain the growth of the two-dimensional columnar vortices in rotating flows around $Ro = 1$, but the mechanisms generating and dominating their robust nonlinear growth in the intermediate-Ro regime in decaying and forced flows remain unclear. Whether the dominant mechanisms leading to two-dimensionalization in forced and decaying flows are similar or distinct also remains unclear. Indeed, the emerging picture in

decaying turbulent flows is that of two-dimensional large-scale columnar vortices characterized by a slow time scale, while inertial waves are characterized by fast time scales and observed to cascade energy downscale. In this framework, clearly the two-dimensional large-scale columnar vortices would quickly contain most of the energy of the system. In forced turbulent flows the problem is different, particularly if one takes the approach of forcing the three-dimensional wave modes only. In this case, it is not obvious that the energy accumulating in the two-dimensional columnar structures should necessarily end up dominating the total energy budget and even less clear that if it did, this would be independent of the scale of energy injection used. We will address this question below after a brief review of the literature on the energy transfers and scaling laws in rotating turbulence.

1.2. *Energy transfers and scaling laws in turbulent rotating flows: observations and theory*

Isotropic spectra of total energy with slopes of ≈ -2 were observed in flows forced in the large scales (e.g. Yeung & Zhou 1998; Thiele & Müller 2009) and reported for scales smaller than the forcing scale l_f for flows forced at intermediate scales (Smith & Waleffe 1999). Thiele & Müller (2009) who forced at large scales reported a horizontal energy spectrum scaling as k^{-2}, but as k^{-3} for the horizontal spectrum for the waves with the larger vertical scales (vertical wavenumber fixed and small). A -3 scaling of energy spectra in rotating flows forced at intermediate scales has been discussed in concomitance with a possible inverse cascade of two-dimensional vortical energy on various occasions. The emerging observed picture involved a combination of downscale cascade of three-dimensional wave energy coexisting with an inverse two-dimensional energy cascade for scales larger than the forcing intermediate scale (e.g Smith & Waleffe 1999; Mininni, Alexakis & Pouquet 2009; Thiele & Müller 2009, and references therein).

Various scaling arguments for rotating flows arrived at slopes for the total energy spectrum ranging from $-5/3$ in the weak rotation regime to -2 for strongly rotating flows (e.g. Zhou 1995; Canuto & Dubovikov 1997). These scaling arguments are inspired by classical theories of homogeneous forced turbulence, starting with Komolgorov's similarity theory (Kolmogorov 1941) assuming that the nonlinear energy transfers involve interactions between modes of similar length scales. In Fourier space this corresponds to triads for which all three wavevector legs are of comparable scale (e.g. Lesieur 1997). The role of non-local triads of helical modes in non-rotating flow was discussed in the context of local vs. non-local energy transfers by e.g. Waleffe (1993) and references therein. In the context of two-dimensionalization of rotating flows, the relative roles of local and non-local wave–vortex energy transfers remains unknown: if one assumes that these are local, then inertial waves forced at scale l_f are expected to exchange energy with waves and vortices of comparable scales. If an inverse cascade of two-dimensional energy and direct cascade of two-dimensional enstrophy are present as conjectured, then a -3 Kraichnan-type slope is expected for the two-dimensional energy spectrum at horizontal scales smaller than l_f, while a $-5/3$ Kolmogorov-type slope would be expected at scales larger than l_f. These features were not observed in the forced rotating flows reported above. Instead, flows forced at intermediate scales did show horizontal energy spectra as steep as -3; however, this was for a range of scales *larger*, not smaller than l_f (e.g. Smith & Waleffe 1999). The different results reported above diverging from the classical analogues of two-dimensional or three-dimensional energy cascades led to the suggestion that the -3 scaling for the energy spectrum in forced rotating three-dimensional turbulence is fundamentally distinct from the scaling of classical

two-dimensional turbulence (e.g. Bellet *et al.* 2006). Clearly, determining the nature of the nonlinear interactions between two-dimensional vortices and three-dimensional waves is key for the proper understanding and modelling of the energy cascades observed in turbulent flows dominated by rotation. The focus of our manuscript is elucidating these processes.

1.3. *Questions and outline*

In the present paper we examine the nature of the nonlinear interactions responsible for generating the columnar structures observed in forced rotating flows. In previous works both two-dimensional and three-dimensional modes were forced at similar scales and the role of the two-dimensional–three-dimensional interactions relative to two-dimensional–two-dimensional interactions remained unknown. By contrast, here we only force the three-dimensional wave modes and extract detailed transfer statistics to clarify the role of the two-dimensional–three-dimensional interactions in generating the dominant two-dimensional columnar structures. We observe that the two-dimensional–three-dimensional interactions lead to the robust columnar structures observed in the forced flows in the intermediate-*Ro* regime. In §2 we present the theoretical background. In §3 we present the numerical approach used. The existence of the intermediate-*Ro* regime is then discussed in §4. The following questions are addressed in the next two sections: (§5) What are the scales and associated local/non-local nature of the dominant two-dimensional–three-dimensional nonlinear interactions at the origin of the accumulation of energy into the large columnar structures of the flow? (§6) Are the dominant nonlinear interactions consistent with an inverse energy cascade mechanism and/or previous scalings found for rotating flows? Contrary to previous forced turbulence studies, we vary the scale of the forcing to determine the robustness. Finally, implications of the results and conclusions are found in §7.

2. Governing equations and modal decomposition

The incompressible equations of motion in a rotating frame are

$$\frac{\partial \boldsymbol{u}}{\partial t} + (\boldsymbol{u} \cdot \nabla)\boldsymbol{u} + 2\Omega \hat{\boldsymbol{z}} \times \boldsymbol{u} = -\nabla p + \boldsymbol{f}(\boldsymbol{u}) + \boldsymbol{D}(\boldsymbol{u}), \quad \nabla \cdot \boldsymbol{u} = 0, \qquad (2.1)$$

where $\boldsymbol{u} = u\hat{\boldsymbol{x}} + v\hat{\boldsymbol{y}} + w\hat{\boldsymbol{z}}$ is the fluctuation component of zero-mean flow, p is the pressure field, $\boldsymbol{f}(\boldsymbol{u})$ and $\boldsymbol{D}(\boldsymbol{u})$ are the forcing and dissipation operators, respectively. They are discussed in further detail in §3. Without loss of generality, we choose the rotation vector to be aligned with the vertical (direction of the unit vector $\hat{\boldsymbol{z}}$). In a periodic domain, the equations of motion of the Fourier transform of the velocity field of a rotating incompressible viscous fluid are

$$\left(\frac{\partial}{\partial t} - \hat{D}(\boldsymbol{k})\right)\hat{u}_n(\boldsymbol{k}, t) + \underbrace{2P_{nj}(\boldsymbol{k})\Omega \epsilon_{j3m}\hat{u}_m(\boldsymbol{k})}_{\textit{Coriolis term}} = -\frac{1}{2}\mathrm{i}\underbrace{\sum_{p|k=p+q} P_{njl}(\boldsymbol{k})\hat{u}_j(\boldsymbol{p}, t)\hat{u}_l(\boldsymbol{q}, t)}_{\textit{Nonlinear term}} + \hat{f}_n(\boldsymbol{k}),$$

$$(2.2)$$

where $\hat{u}_n$ is the Fourier transform of the nth-component of the velocity field, $\boldsymbol{k}$ is the wavenumber, $\hat{D}(\boldsymbol{k})$ and $\hat{f}_n(\boldsymbol{k})$ are the Fourier transforms of the dissipation and forcing operators, respectively, ϵ_{ijk} is the alternating tensor and $P_{njl}(\boldsymbol{k}) = k_l P_{nj} + k_j P_{nl}$ with $P_{nj} = \delta_{nj} - k_n k_j / k^2$ are the classical projection operators onto a plane perpendicular to $\boldsymbol{k}$ accounting for the non-divergence of the incompressible flow. Finally, δ_{nm} is
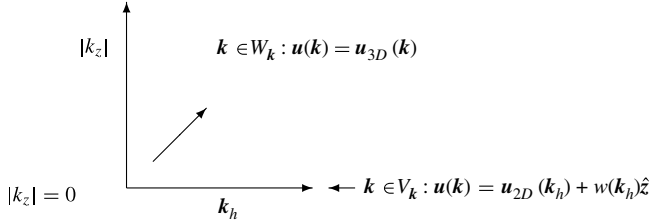
FIGURE 1. Decomposition of the Fourier modes onto V_k and W_k modes defined by (2.5).

the Kronecker delta, and n, m and j are dummy indices taking values of 1, 2 and 3. From (2.2), the equation governing the energy spectrum $E(\boldsymbol{k}, t) = \frac{1}{2}|\hat{\boldsymbol{u}}(\boldsymbol{k}, t)|^2$ is

$$\left(\frac{\partial}{\partial t} - 2\hat{D}(\boldsymbol{k})\right) E(\boldsymbol{k}, t) = T(\boldsymbol{k}, t) + \underbrace{\mathrm{Re}[\hat{u}_n^*(\boldsymbol{k})\hat{f}_n(\boldsymbol{k})]}_{Energy\ input\ F} \quad (2.3)$$

where * stands for complex conjugate, Re denotes the real part, and $T(\boldsymbol{k}, t)$ is the energy transfer spectrum for the Fourier component of wavenumber $\boldsymbol{k}$ quantifying the energy exchange between the interacting triads of Fourier wavenumbers satisfying $\boldsymbol{k} = \boldsymbol{p} + \boldsymbol{q}$:

$$T(\boldsymbol{k}, t) = \sum_{\boldsymbol{p}|\boldsymbol{k}=\boldsymbol{p}+\boldsymbol{q}} T(\boldsymbol{u}_k|\boldsymbol{u}_p, \boldsymbol{u}_q) = \frac{1}{2}\mathrm{Im}\left[\sum_{\boldsymbol{p}|\boldsymbol{k}=\boldsymbol{p}+\boldsymbol{q}} \hat{u}_n^*(\boldsymbol{k}, t)P_{njl}(\boldsymbol{k})\hat{u}_j(\boldsymbol{p}, t)\hat{u}_l(\boldsymbol{q}, t)\right], \quad (2.4)$$

where Im denotes the imaginary part. The focus of this study is on the particular case of rotating flows in the intermediate-Rossby-number regime known to be dominated by columnar zero-frequency vortices; we thus proceed to further decompose the statistics of the flow in terms of its wave and vortical components.

2.1. *Vortical and wave modes: two-dimensional and three-dimensional dynamics*

The separation between the dynamics of the modes with non-zero and zero inertial wave frequencies was observed in previous studies of rotating flows (e.g. Chen *et al.* 2005; Bourouiba 2008*b*; Thiele & Müller 2009) and discussed (e.g. Babin, Mahalov & Nicolaenko 2000) for highly rotating flows. It is then natural to follow the analysis of such flows in terms of these two major classes of modes: the wave three-dimensional modes with non-zero linear inertial wave frequencies ($k_z \neq 0$) and the vortical zero-frequency modes ($k_z = 0$) as illustrated in figure 1:

$$\text{If } \boldsymbol{k} \in V_k = \{\boldsymbol{k} \mid \boldsymbol{k} \neq 0 \text{ and } k_z = 0\} \text{ then } \boldsymbol{u}(\boldsymbol{k}) = \boldsymbol{u}_{2D}(\boldsymbol{k}_h) + w(\boldsymbol{k}_h)\hat{z}, \quad (2.5)$$

$$\text{If } \boldsymbol{k} \in W_k = \{\boldsymbol{k} \mid \boldsymbol{k} \neq 0 \text{ and } k_z \neq 0\} \text{ then } \boldsymbol{u}(\boldsymbol{k}) = \boldsymbol{u}_{3D}(\boldsymbol{k}), \quad (2.6)$$

where the vortical modes describe the two-dimensional part of the velocity field independent of the vertical direction. This two-dimensional field is separated into a two-component horizontal part $\boldsymbol{u}_{2D}$ and a vertical velocity part $w\hat{z}$. The energy contributions are then decomposed into three types of modes: $E = E_{3D} + E_{2D} + E_w$, where $E_{2D} = \frac{1}{2}\sum_{\boldsymbol{k}\in V_k}|\boldsymbol{u}_{2D}(\boldsymbol{k})|^2$, $E_w = \frac{1}{2}\sum_{\boldsymbol{k}\in V_k}|w(\boldsymbol{k})|^2$, and $E_{3D} = \frac{1}{2}\sum_{\boldsymbol{k}\in W_k}|\boldsymbol{u}_{3D}(\boldsymbol{k})|^2$. Using this decomposition, the spectral energy budgets can be written as

$$\left(\frac{\partial}{\partial t} - \hat{D}_{W_k}\right) E_{3D}(\boldsymbol{k} \in W_k) = (F + T_{33\to3} + T_{32\to3} + T_{3w\to3})(\boldsymbol{k} \in W_k), \quad (2.7)$$

$$\left(\frac{\partial}{\partial t} - \hat{D}_{V_k}\right) E_{2D}(\boldsymbol{k} \in V_{\boldsymbol{k}}) = (T_{22 \to 2} + T_{33 \to 2})(\boldsymbol{k} \in V_{\boldsymbol{k}}), \tag{2.8}$$

$$\left(\frac{\partial}{\partial t} - \hat{D}_{V_k}\right) E_w(\boldsymbol{k} \in V_{\boldsymbol{k}}) = (T_{2w \to w} + T_{33 \to w})(\boldsymbol{k} \in V_{\boldsymbol{k}}), \tag{2.9}$$

where the Fourier transform of the dissipation operator is also split between equations, which is discussed in the next section. The input of energy, $F(\boldsymbol{k})$, into wavemodes $\boldsymbol{k}$ only appears in the three-dimensional equation as explained earlier. The transfer spectra account for detailed interactions between modes of various types. For example $T_{33 \to 2}(\boldsymbol{k}_h \text{ or } \boldsymbol{k} \in V_{\boldsymbol{k}})$ stands for transfers involving triads in which two three-dimensional wave modes are exchanging energy with two-dimensional vortical modes. Following the notation introduced in (2.4), this is written

$$T_{33 \to 2}(\boldsymbol{k} \in V_{\boldsymbol{k}}, t) = \sum_{\boldsymbol{p},\boldsymbol{q} \in W_{\boldsymbol{k}} | \boldsymbol{k}=\boldsymbol{q}+\boldsymbol{p}} T(\boldsymbol{u}_{2D\boldsymbol{k}} | \boldsymbol{u}_{3D\boldsymbol{p}} \boldsymbol{u}_{3D\boldsymbol{q}}). \tag{2.10}$$

Similarly, the other types of transfers are defined according to the contribution of each category of mode. Note that the $T_{jk \to i}$ terms are symmetric in j and k. Note also from (2.7)–(2.9) that energy in the two-dimensional modes E_{2D} can only grow in association with nonlinear transfers of the type $33 \to 2$. We also define the two-dimensional enstrophy only associated with the two-dimensional $V_{\boldsymbol{k}}$ modes as

$$V_{2D} = \sum_{\boldsymbol{k} \in V_{\boldsymbol{k}}} V_{2D}(\boldsymbol{k}) = \sum_{k_h \in [1 \ k_t]} k_h^2 E_{2D}(k_h) = \frac{1}{2} \sum_{\boldsymbol{k} \in V_{\boldsymbol{k}}} |\omega_z(\boldsymbol{k})|^2, \tag{2.11}$$

where ω_z is the vertical component of the vorticity vector.

3. Numerical approach and forcing schemes

The equations were solved using a standard pseudo-spectral method in a triply periodic cubic domain of length 2π. The leapfrog scheme with Asselin–Robert filter to control the computational mode (Asselin 1972) was used for time differencing. The highest value of the filter parameter was 0.035. The Coriolis parameter 2Ω was fixed at $2\Omega = 22.6 \text{ s}^{-1}$. The 2/3 rule was used for de-aliasing, with $k_{truncation} = N/3$, where N^3 is the resolution (Boyd 1989). The anisotropy of the rotating problem favours the use of cylindrical truncation of the Fourier modes. The horizontal and vertical components of the statistics are examined separately rather than using a spherical truncation and isotropic spectra and statistics which are more appropriate for the study of isotropic turbulence. The cylindrical truncation and associated dissipation operator are defined as $|k_z| = |k_h| = k_{truncation}$, where $k_h = \sqrt{k_x^2 + k_y^2}$ and $\boldsymbol{D} = (-1)^{n+1} \nu_n (\nabla_h^{2n} + (\partial/\partial z)^{2n})$, where ∇_h is the horizontal nabla operator. An eighth-order cylindrical hyperviscosity operator with $n = 4$ is applied leading to $\hat{D} = -\nu[(k_x^2 + k_y^2)^4 + k_z^8]$ in Fourier space with $\hat{D}_{V_k} = -\nu (k_x^2 + k_y^2)^4$ and $\hat{D}_{W_k} = -\nu[(k_x^2 + k_y^2)^4 + k_z^8]$. No additional large-scale damping is applied. The viscosity coefficient, ν, is given in subsequent sections.

Following an initial spin-up, a quasi-equilibrium is reached. That is, although two-dimensional energy is observed to continue to grow, other statistics, such as the three-dimensional energy spectrum and spectral transfers, stabilize. The forcing function in the nth component of the three-dimensional wave velocity field is

$$\hat{f}_n(\boldsymbol{k}, t) = \epsilon(\boldsymbol{k})/u_n^*(\boldsymbol{k}, t), \tag{3.1}$$

Forcing type	$\epsilon(\boldsymbol{k})$	k_h	k_z	Resolution
F1	$a_1(28 - k_h)(k_h - 26)$	[26 28]	$\neq 0$	128^3
F2	$a_2(28 - k_z)(k_z - 32)/k_h^2$		[28 32]	128^3
F3	$a_3(42 - k_h)(k_h - 39)$	[39 42]	$\neq 0$	200^3
F4	$a_4(5 - k_h)(k_h - 2)/k_h^2$	[2 5]	$\neq 0$	200^3
F5	$a_5(108 - k_h)(k_h - 100)$	[100 108]	$\neq 0$	512^3
F6	$a_6(5 - k_h)(k_h - 2)/k_h^2$	[2 5]	$\neq 0$	512^3

TABLE 1. Types of forcing used. The total input of energy F at each time step is roughly constant. The amplitudes a_j with $j = 1$–6 are varied to obtain different levels of forcing, F (see Appendix). The values of a_{3-6} were chosen to obtain a steady value of $Ro \approx 0.2$ in each simulation, leading to $(a_3, a_4, a_5, a_6) = (1 \times 10^{-6}, 0.8 \times 10^{-5}, 5 \times 10^{-11}, 1 \times 10^{-7})$.

where $u_n^*(\boldsymbol{k}, t)$ is the complex conjugate of the nth Fourier component of the velocity vector. The advantage of this forcing is that the total energy input $F = \sum_{\boldsymbol{k}} \mathrm{Re}[\hat{u}_n^*(\boldsymbol{k}) \hat{f}_n(\boldsymbol{k})] = 3 \sum_{\boldsymbol{k}} \epsilon(\boldsymbol{k})$ is constant throughout the simulation so that the changes and accumulation of the levels of energy at certain scales are only due to the dynamics and easily traceable. Note that we take the divergence-free part of the forcing. The scales of the modes forced are described by $\epsilon(\boldsymbol{k})$ detailed in table 1. Unless otherwise indicated, Ro is calculated based on the vertical component of the entire vorticity field, $\boldsymbol{\omega} = \nabla \times \boldsymbol{u}$. Then $Ro = \sqrt{[\omega_z^2]}/(2\Omega)$.

The resolutions used are 128^3, 200^3, and 512^3. The first two have the advantage of allowing us to perform a large range of simulations (e.g. 30 simulations as discussed in the paper and Appendix) and observe the dynamics for a long time. The last was used to check the robustness of the results to the increase of resolution, which is clearly confirmed. Our focus is on the clarification of the role of the nonlinear interactions between waves and vortices in the two-dimensionalization of rotating forced flows. All the resolutions used ensure the existence of the interactions known to be important for the key nonlinear triad interactions in rotating flows in the intermediate-Ro regime as was shown in Bourouiba (2008a). All 128^3 and 200^3 simulations were initiated with a total seed energy of ≈ 0.01. The 512^3 simulations were initiated with a total seed energy of $\approx 1 \times 10^{-5}$.

4. The intermediate-Ro regime in forced flows

We begin with a series of 128^3 simulations using F1 and F2 spanning a range of Rossby numbers between ≈ 1.5 and $\approx 8 \times 10^{-2}$. The full range of parameters used are given in the table in the Appendix. Different Ro were achieved by varying the strength of the forcing. Except in our higher-Ro simulations, true statistical stationarity was not reached. However, beyond $t = 65$, other statistics (e.g. Ro and T_{23}) did appear to reach statistical stationary (not shown). For smaller and intermediate values of Ro, E_{2D}/E continued to grow throughout the simulation, leading to an increase of the total energy, while E_{3D}/E decreased with time for all simulations in the intermediate-Ro range for all forcings (see examples of normalized time series for F1 in figure 2a,b).

A useful measure of the coupling between two-dimensional and three-dimensional modes is the time-averaged cumulative energy transfer between the three-dimensional
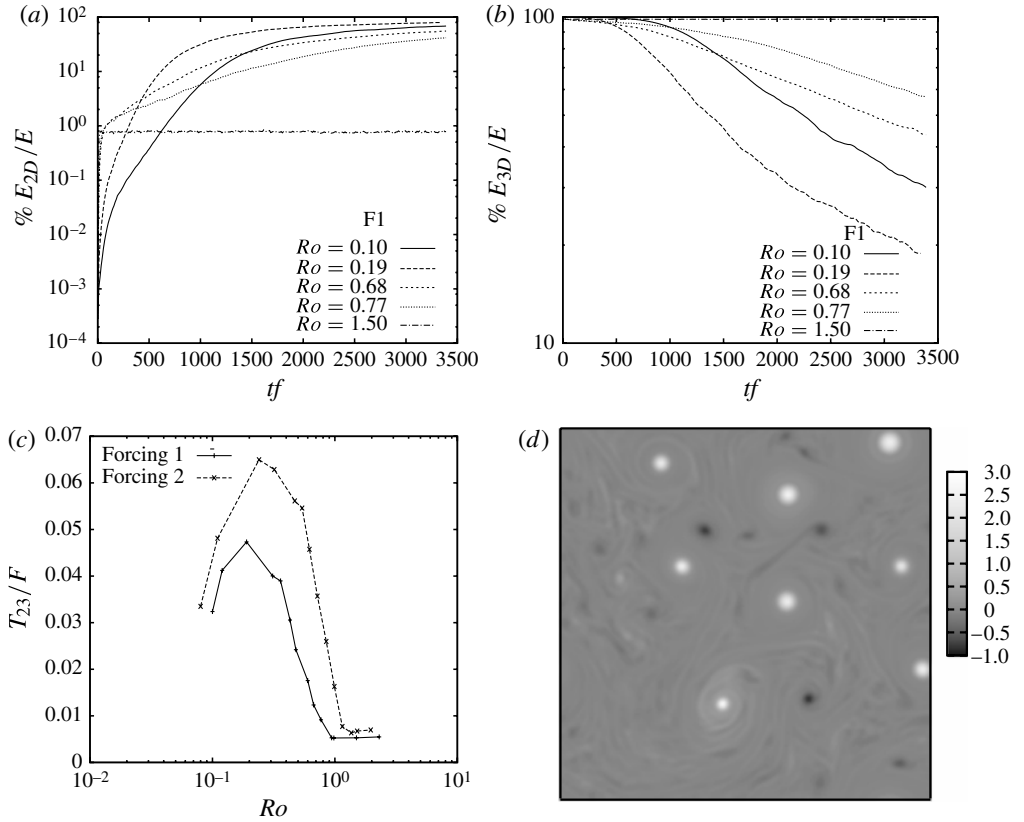
FIGURE 2. Top: time series of (*a*) E_{2D}/E and (*b*) E_{3D}/E for flow forced by F1. Bottom: (*c*) integrated transfer $\overline{T_{23}/F}(Ro)$ shown as a function of the Rossby number for simulations forced with forcings F1 and F2; (*d*) snapshot of the total vorticity field for a simulation in the intermediate-*Ro* range forced by forcing F4 at 200^3, shown at time $t = 142.5$ and normalized by the Coriolis parameter ($f = 2\Omega = 22.6\ \text{s}^{-1}$).

and the two-dimensional modes:

$$\bar{T}_{23}(Ro) = \sum_{k \in V_k} \bar{T}_{33 \rightarrow 2}(\boldsymbol{k}, Ro), \qquad (4.1)$$

where the overbar denotes the time-average.

Figure 2(*c*) shows the *Ro* dependence of time averages of total T_{23} normalized by the corresponding F and averaged over the time window $t \in [65\ 125]$. Clearly the cumulative energy exchange between the two-dimensional and the three-dimensional modes is positive and peaks at intermediate $Ro = 0.19$. The quantity is positive indicating an overall injection of energy from the waves to the vortices. This is observed for both F1 and F2, which are forcing the inertial waves in small and large horizontal (and small vertical) scales, respectively. This result is reminiscent of the intermediate-*Ro* regime identified in decaying rotating turbulence in Bourouiba & Bartello (2007). Figure 2(*d*) shows a snapshot of the vorticity field for the simulation at higher resolution forced with F4 at large horizontal scales and for which *Ro* is chosen to be in the intermediate regime. We observe the appearance
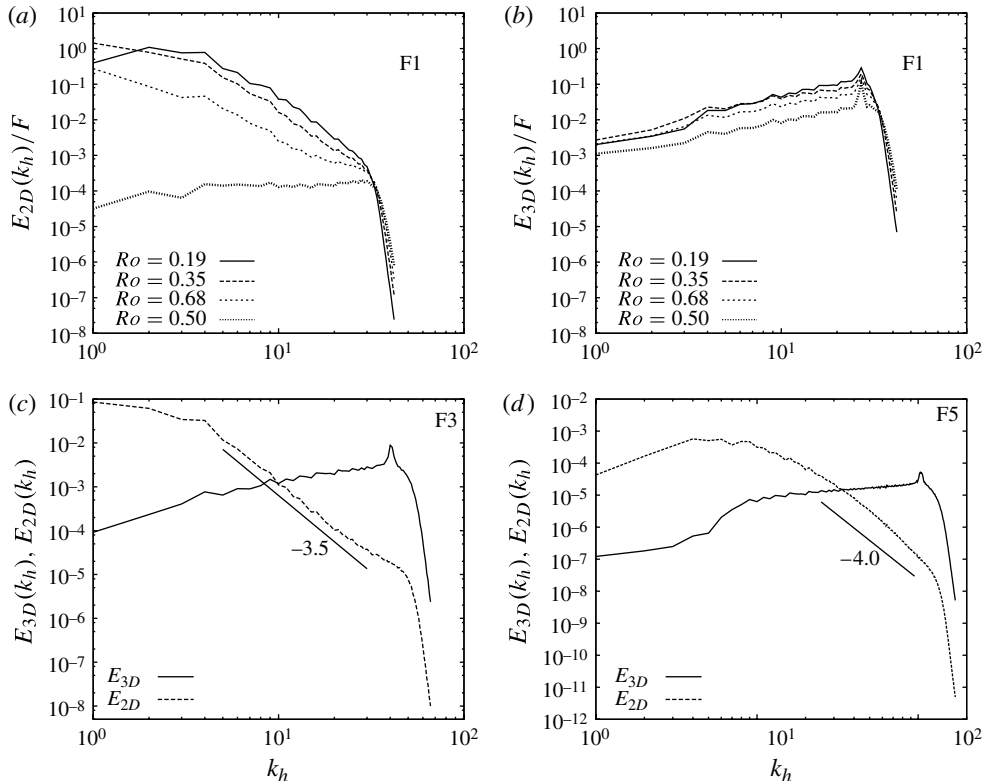
FIGURE 3. Top: time-averaged horizontal energy spectra normalized by the input of energy F averaged on $t \in [65\ 85]$ showing (*a*) the energy in the two-dimensional modes and (*b*) the energy in the three-dimensional wave modes when the flow is forced by F1. Bottom: time-averaged spectra in $t \in [100\ 125]$ $E_{2D}(k_h)$, $E_{3D}(k_h)$ for the flows forced with (*c*) F3, 200^3 and (*d*) F5, 512^3.

of the dominant vortices in this flow as well (snapshots for F1 and F2, not shown) with a marked cyclone–anticyclone asymmetry, showing clearly that the two-dimensional–three-dimensional interactions are forcing the vortical modes. Indeed recall that previous simulations used a forcing of both two-dimensional and three-dimensional modes, hence the presence of the intermediate-*Ro* regime for such forced flows and the dominant nature of the two-dimensional–three-dimensional interactions over directly forced two-dimensional–two-dimensional interactions was not determined. Here, we showed its existence and robustness to change of forcing scale of the three-dimensional modes. As noted previously, the only input of energy into the two-dimensional modes in these simulations originates from the term (2.10) in (2.8). We now focus on the characterization of the key three-dimensional–two-dimensional nonlinear interactions identified to be at the origin of the increase of vortical energy E_{2D} observed.

It is useful to first consider the horizontal energy spectra of both waves and vortices (e.g. figure 3*a*,*b*). In the lower-resolution simulations, the time-averaged spectra in the high-*Ro* regime are not significantly affected by rotation for either forcing type. That is, the $E_{2D}(k_h)$ and $E_{3D}(k_h)$ spectra have shapes similar both to one another and to what one would expect for isotropic turbulence. As *Ro* decreases, $E_{2D}(k_h)$ increases

markedly at large scales and a steepening of the spectral slope results. This becomes more pronounced as *Ro* decreases down towards 0.2, below which the trend reverses as seen for example for the simulations forced with F1 in figure 3(*a,b*). Similar spectra for the 200^3 and 512^3 simulation using F3 and F5, which are analogous to forcing F1 at 128^3, are shown in figure 3(*c,d*). The $E_{3D}(k_h)$ are peaked near the forcing scale and have positive slopes. The $E_{2D}(k_h)$ have a peak at about $k_h = 3$–4 and slopes steeper than -3. Note that much longer simulations at 200^3 resolution suggest that the peak 'condensates' onto the gravest k_h increases in the long time limit (not shown).

5. Local or non-local dominant two-dimensional–three-dimensional energy transfers?

We next focus on a more detailed description of $T_{33\rightarrow2}(k_h, t)$ in the intermediate-*Ro* regime, where the overall $T_{23}(Ro)$ is the strongest. For this, we use 200^3 and 512^3 resolutions with forcing schemes (F3, F4) and (F5, F6), respectively. The forcing amplitudes were tuned so that $Ro \sim 0.2$.

We wish to better describe the $33 \rightarrow 2$ transfers. In particular, are the dominant nonlinear energy transfers between three-dimensional and two-dimensional modes identified to be at the origin of the intermediate-*Ro* regime local or non-local in scale? Recall that in isotropic three-dimensional turbulence, a triad of modes p, q, k with $k + p + q = 0$ is typically said to be *local* if $s \leqslant 2$ and *non-local* if $s \geqslant 2$, where $s(k, p, q) = \max(k, p, q)/\min(k, p, q)$ (e.g. Zhou 1993*a,b*; Lesieur 1997; Domaradzki & Carati 2007). Stricter definitions can also be found. These include requiring the ratio between the middle-to-smaller or larger-to-middle wavenumbers to be greater than 2 (e.g. Domaradski 1988). In two-dimensional turbulence, a ratio of the largest-to-smallest leg of the triad larger than 4 (e.g. Watanabe & Shepherd 2001) was used to define non-locality. One also needs to distinguish between local triads and local transfers. A local interaction (via local triad) can only be responsible for a local energy transfer; however, a non-local triad can lead to both local and non-local energy transfers.

In our problem, recall that $T_{33\rightarrow2}(k)$ measures the energy exchange between a given two-dimensional mode of wavevector $k \in V_k$ and all the combinations of pairs of three-dimensional modes $(p, q) \in W_k$ such that $p + q = k$. For these triads, this equation implies that the vertical components of the wavenumbers q and p are equal in magnitude and have opposite signs, i.e. $q_z = -p_z$. In order to address the non-local/local nature of the $33 \rightarrow 2$ triads and energy transfers we use this fact to further decompose the energy spectra $T_{33\rightarrow2}(k)$ based on the scale of the horizontal wavenumbers q_h, p_h, k_h involved in the injection of energy into the two-dimensional vortical modes. We proceed by classifying the horizontal scales into three main disjoint regions A, B, and C. These correspond to small, medium and high horizontal wavenumbers, respectively. The $T_{33\rightarrow2}(k \in V_k)$ transfer into the modes $(k_h, 0)$ is then the sum of contributions from the wave modes for which the legs (q_h and p_h) both lie in A, both in B, both in C, one in A and one in B, etc. We will refer to these various contributions as AA, BB, CC, AB, AC, and BC. For example, $T_{33\rightarrow2}^{AB}(k_{2D}|p_{3D}, q_{3D})$ has either p_{3D} or q_{3D} in A and the other in B, with an overall contribution

$$T_{33\rightarrow2}^{AB}(k \in V_k) = \sum_{p, q \in W_k | k=q+p} T(u_{k \in V_k}|u_{p \in A}, u_{q \in B}). \tag{5.1}$$

The boundaries between the regions are chosen so that the *stricter* definition of non-locality can be detected, i.e. there is a ratio of at least 2 between all k_h in C and all
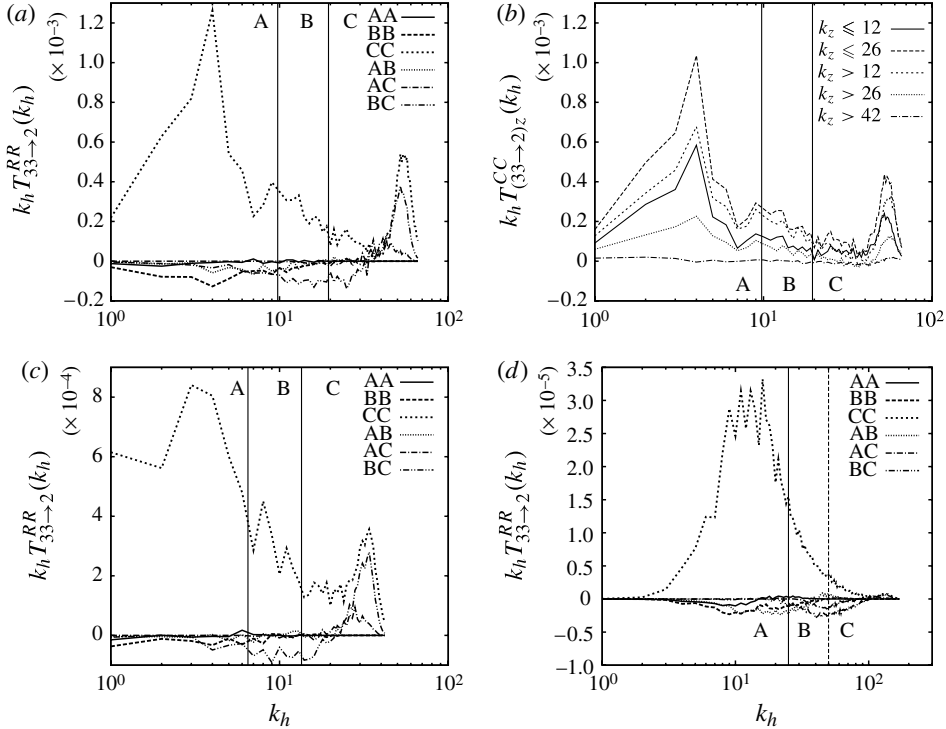
FIGURE 4. Detailed time-averaged horizontal energy transfer spectra for forcing schemes at the small horizontal scales. (*a*) $T_{33\to2}^{RR}(k_h)$ defined in (5.1) for flow forced with F3 (200^3). R is either region A or B or C. $T_{33\to2}^{AA}(k_h)$, $T_{33\to2}^{BB}(k_h)$, $T_{33\to2}^{CC}(k_h)$, $T_{33\to2}^{AB}(k_h)$, $T_{33\to2}^{AC}(k_h)$, $T_{33\to2}^{BC}(k_h)$ are labelled AA, BB, CC, AB, AC, and BC, respectively. The vertical lines mark the borders between the disjoint regions A, B, and C. (*b*) $T_{33\to2}^{CC}(k_h)$ averaged between $t = 100$ and $t = 125$ and filtered according to the vertical wavenumber $|k_z|$ of the three-dimensional modes. Bottom: same as (*a*), but for (*c*) the lowest resolution 128^3 and forcing F1 and (*d*) the highest resolutions 512^3 and forcing F5.

in A. Moreover, the limit between region C and B is chosen to ensure that a ratio of at least 2 is satisfied between the small-scale *forced* modes and the boundary of region B. For example, at 200^3, the boundary between A and B was chosen as $k_h = 9.75$ and between B and C as $k_h = 19.5$, ensuring that the forced modes $k_h \in [39\ 42]$ (F3) in region C are at least twice as large as the k_h of all the modes in region B. Similarly for 512^3 (128^3) F5 (F1) with forced modes $k_h \in [100\ 108]$ ($k_h \in [26\ 28]$), leading to a boundary between A and B at $k_h = 25$ ($k_h = 6.5$) and between B and C at $k_h = 50$ ($k_h = 13$).

Figure 4(*a*) compares the time-averaged contributions to $T_{33\to2}(k_h)$ for the 200^3 simulation forced with F3. These are also compared to the results obtained from the lower resolution 128^3 forced with F1 and the highest resolutions 512^3 forced with F5. Positive values at a given k_h correspond to three-dimensional modes adding energy into two-dimensional modes at that k_h. Thus, for example, in region A, the curve denoted AA corresponds to $33 \to 2$ transfers of type AA $\to$ A, in which all three modes of the triad are in region A. In region B, the same curve corresponds to AA $\to$ B transfers, in which the two three-dimensional modes are in region A and the two-dimensional mode of the triad is in region B. From the figure, we

conclude that $T_{33 \to 2}(k_h)$ is clearly dominated by the energetic contribution of triads of type $CC \to A$. This is also the case for smaller resolutions with forcing in the small horizontal scales (F1) and larger resolutions with forcing also in the small horizontal scales (F5) shown in figures 4(c) and 4(d), respectively. Figure 4(b) shows $T^{CC}_{33 \to 2}(k_h)$ after a further filtering according to the vertical wavenumber of the two three-dimensional modes. Most of the $33 \to 2$ energy transfer of type $CC \to A$ is seen to involve three-dimensional wave modes with vertical wavenumbers, $|k_z| \leqslant 26$. These are modes with relatively small linear frequencies ω_k. From both graphs, it is evident that the substantial portion of the energy transfers from triads $33 \to 2$ are from three-dimensional modes with $k_h > 20$ and $|k_z| \leqslant 26$ to two-dimensional modes with $k_h \sim 3$–4. By classical definitions, such triads and energy transfers are clearly *non-local*.

That the non-local $CC \to A$ transfers should be dominant is odd in that one would normally expect $33 \to 2$ exchanges to be between like horizontal scales, i.e. in local triads as observed in isotropic turbulence. Is it simply that most of the transfer is from the forced three-dimensional modes (which happen to be in region C for F1, F5) directly into the large k_h scales of region A?

To address this last point, we considered a series of simulations of increasing resolution all forced in the large scales (small k_h). We use F2 at 128^3, F4 at 200^3, and F6 at 512^3. If the non-locality observed above is an artifact of the small three-dimensional scale forcing and a large concentration of energy in the larger horizontal two-dimensional columnar vortices, then the new F2, F4, F6 large three-dimensional scale forcings should lead to dominant local interactions of type $AA \to A$. In fact, these three forcings would allow local in scale $AA \to A$ interactions to dominate the signal of an *artificial* non-local three-dimensional-to-two-dimensional energy transfer mechanisms of type $CC \to A$. The horizontal energy transfer spectra for these simulations are shown in figure 5. As with the forcing in small horizontal scales F1, F3, and F5, the $33 \to 2$ energy transfers for F2, F4, and F6 are dominated by energy exchanges of type $CC \to A$, which are again non-local. The increase of resolution to 512^3 with forcing F6 shows clearly the robustness of this characteristic non-locality. The non-locality is robust and not induced by a particular forcing in region C. The mechanism of two-dimensionalization in homogeneous rotating turbulence clearly appears to involve a direct injection of energy from the small frequencies elongated three-dimensional wave modes (large vertical scales) into the larger columnar two-dimensional structures of the flow. This is in contrast to the more classical view whereby energy injected into two-dimensional modes at smaller scales, locally, would cascade to larger scales in association with two-dimensional vortical dynamics and a $-5/3$ energy spectrum.

6. Discussion of the two-dimensional dynamics

Recall from figure 3 that for the intermediate values of Ro of interest here, $E_{2D}(k_h)$ has slopes greater than -3 (also observed for simulations with higher resolution in the present work and other works (e.g. Smith & Waleffe 1999; Chen *et al.* 2005)). Similar spectral slopes are also familiar in classical two-dimensional turbulence; however, there, the ≈ -3 slopes are to the right of the forcing scale, whereas here they are to the left. Nevertheless, although the ≈ -3 slope lies to the left of the (three-dimensional) forcing in our simulations, we showed that it particularly lies to the right of where the bulk of the $33 \to 2$ energy is injected into the two-dimensional modes occurs. As such, the ≈ -3 slope observed to the left of the forcing in
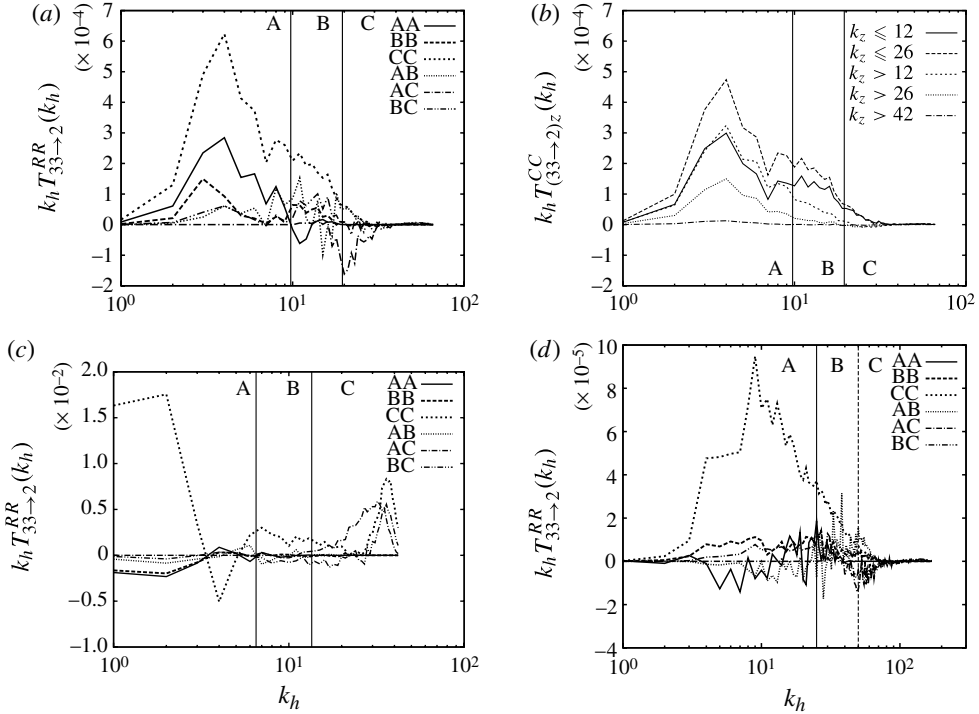
FIGURE 5. Detailed time-averaged horizontal energy transfer spectra for forcing schemes at the large horizontal scales. (*a,b*) Same as figure 4 for the 200^3 flow forced in the large horizontal scales using F4 (time averages taken for *t* between 100 and 125). Bottom: same as(*a*), but for the (*c*) the lowest resolution 128^3 and forcing F2 and (*d*) highest resolutions 512^3 and forcing F6.

rotating turbulence (e.g. Chen *et al.* 2005) need not be associated with an inverse cascade of two-dimensional energy. Instead, it is more natural to think of the two-dimensional modes as 'forced' at the large scale (e.g. by $T_{33\to2}$) and of the ≈ -3 slope as associated with a downscale enstrophy transfer. Indeed, recall that the two-dimensional mode dynamics is governed by (2.8) which can be shown to conserve both energy E_{2D} and two-dimensional enstrophy V_{2D} in the limit of large rotation rate (Bourouiba 2008*b*). Moreover, if one considers the term $T_{33\to2}$ as a forcing, then (2.8) becomes the analogue of that governing forced classical two-dimensional turbulence. It is then natural to consider the possibility of enstrophy cascade in the regimes where the two-dimensional/three-dimensional mode decomposition is valid (intermediate- and small-*Ro* regimes).

The two-dimensional enstrophy transfers are displayed for the 200^3 and 512^3 simulations forced in medium to small scales F3 and F5 in figures 6 and 7, respectively. Clearly, the energy injected into the large scales directly by the non-local $33 \to 2$ interactions is in turn transferred to even larger vortical scales by the vortex–vortex interactions $22 \to 2$ (panels *a*). The enstrophy injected into the two-dimensional modes by the $33 \to 2$ nonlinear interactions is transferred from the injection scale to higher dissipation scales by vortex–vortex interactions $22 \to 2$ interactions as well (panels *b*). The interactions of type $33 \to w$ feed E_w at medium to large scales and the $2w \to w$ interactions transfer this energy downscale to the
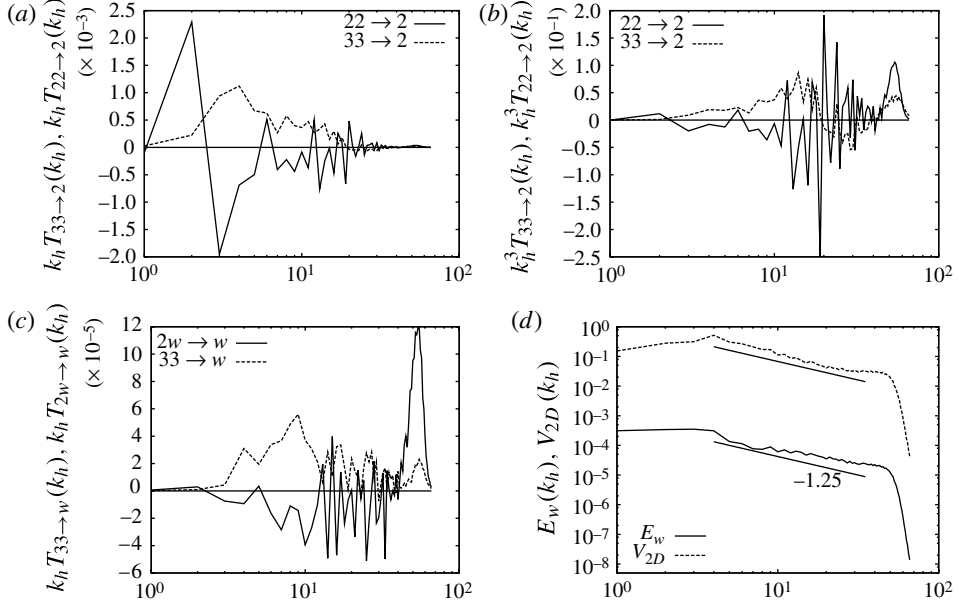
FIGURE 6. Transfer spectra of two-dimensional energy, two-dimensional enstrophy V_{2D} and E_w and and spectra of $E_w(k_h)$ and $V_{2D}(k_h)$ for a flow forced with F3 at 200^3. $t \in [100 \ 125]$
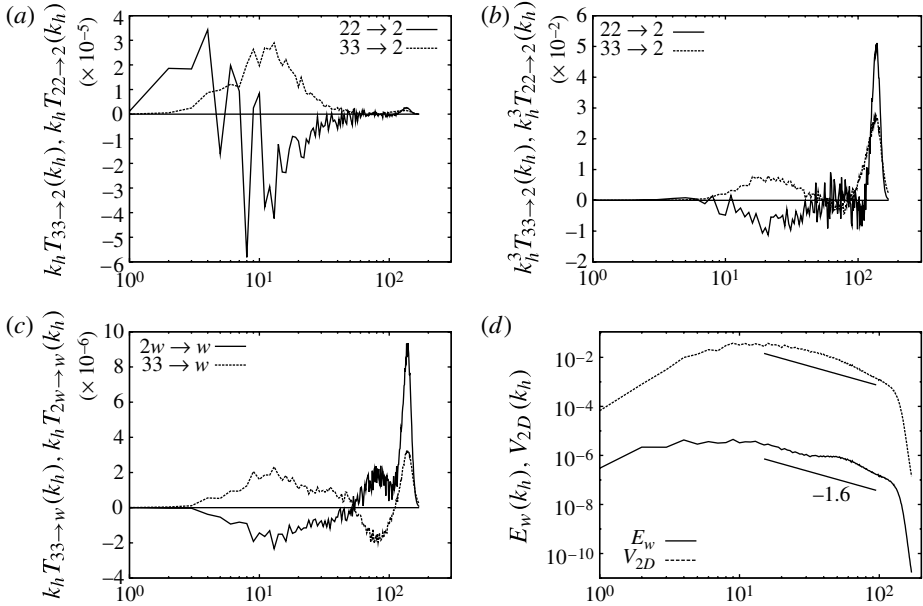

FIGURE 7. Transfer spectra of two-dimensional energy, two-dimensional enstrophy V_{2D} and E_w and and spectra of $E_w(k_h)$ and $V_{2D}(k_h)$ for a flow forced with F5 at 512^3. $t \in [100 \ 125]$

dissipation (panels *c*). Finally, the spectra of V_{2D} and E_w both have slopes close to or steeper than -1 in the range of k_h over which V_{2D} and E_w are transferred downscale (panels *d*). These findings are consistent with what would be expected for a passive
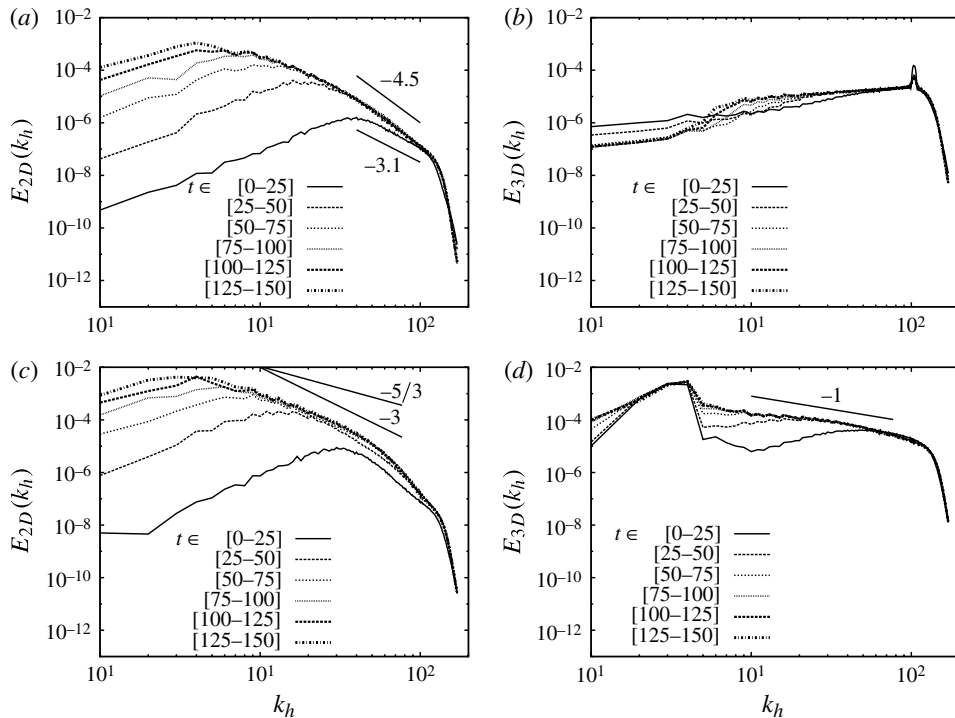
FIGURE 8. Time evolution of (left) two-dimensional energy spectra and (right) three-dimensional energy spectra for forcing in the (*a,b*) small scales F5 and (*c,d*) large scales F6.

scalar w advected in a forced two-dimensional turbulent flow (Lesieur 1997). The increase of resolution confirmed the robustness of these findings as well.

Finally, one could argue that local energy transfers might be hidden by non-local interactions associated with the steep two-dimensional energy spectrum. In this case, one might anticipate a $-5/3$ two-dimensional energy spectrum to appear early on and to steepen to a -3 slope as finite box size effects become relevant. For example a -3 or steeper spectrum was observed in classical two-dimensional turbulence with no large-scale dissipation (e.g. Chertkov *et al.* 2007). In order to test this latter scenario, we examine the time evolution of the two-dimensional energy spectra. Figure 8(*a,b*) shows the energy spectra obtained with the small-scale forcing F5 at 512^3 averaged over a series of time intervals. Clearly, the emergence of the steep spectrum of two-dimensional energy appears early in the temporal flow evolution, prior to any possible influence of a condensate or influence of the larger scales of the finite domain. In figure 8(*c,d*), we finish our discussion with the time evolution for the forcing F6 in large horizontal scales. Once again, we confirm the early emergence of the steep two-dimensional spectra associated with the dominant direct injection of energy via non-local $CC \rightarrow A$ interactions even when local interactions with the forcing scale in region A could have been favoured.

7. Summary and conclusion

We presented the results of a study of forced rotating turbulence over a range of *Ro* and with various resolutions and forcing scales. The focus of the work was on

nonlinear energy transfers between inertial waves and the two-dimensional columnar vortices that are known to emerge in strongly rotating flows. Using numerical experiments and detailed energy transfers we observe that the two-dimensional–three-dimensional interactions lead to the robust columnar structures observed in forced flows and to the existence of the intermediate-*Ro* regime. We then addressed the following questions. (*a*) What are the scales and associated local/non-local nature of the dominant two-dimensional–three-dimensional nonlinear interactions at the origin of the accumulation of energy into the large columnar structures of the flow? (*b*) Are the dominant nonlinear interactions consistent with an inverse energy cascade mechanism and/or previous scalings found for rotating flows? In contrast to previous studies, only the three-dimensional wave modes were forced directly here; as such, all energy in the two-dimensional modes resulted from wave–vortex (two-dimensional–three-dimensional) nonlinear interactions and energy transfers. The following points summarize our findings.

  (i) We confirmed that an intermediate-*Ro* range similar to that seen previously in decaying simulations of rotating turbulence also emerges in sustained flows even if the forcing is only applied to the wave modes.

 (ii) We showed that most of the energy transfers leading to the growth of the two-dimensional columnar vortices in the intermediate-*Ro* regime are carried out by non-local (in scale) interactions. They involve two wave modes with small horizontal scales and small frequency and a large horizontal columnar vortex mode. These non-local triads are responsible for non-local energy transfers in favour of the two-dimensional vortices. They dominate the energy transfers even when local wave–vortex interactions are favoured by forcing configurations.

(iii) We examined the implications of non-locality. The direct injection of energy into large-horizontal-scale vortical modes suggested the possibility of interpreting the steep slope observed in simulations of rotating turbulence in terms of a two-dimensional enstrophy cascade, and not in terms of an inverse cascade mechanism specific to rotating flows. Instead, the two-dimensional dynamics of forced rotating flows in the intermediate-Rossby-number regime could be better thought of as analogous to two-dimensional flow forced at its largest scales.

(iv) We showed that roughly doubling the resolution twice and changing the scale of the forcing does not modify the strong non-local signal captured by the detailed transfer spectra. The dominant non-locality of wave–vortex interactions at the origin of the growth of the vortices and steep two-dimensional energy spectra consistent with a downscale transfer of two-dimensional enstrophy is robust.

In sum, the following picture for the dynamics of the intermediate-*Ro* range in forced flows appears to emerge: regardless of the scale of the forcing, three-dimensional waves of small linear inertial frequency *and* small horizontal scale preferentially interact with larger horizontal two-dimensional vortices, injecting energy into these directly and despite the clear non-locality in scale. The image of local transfers of three-dimensional to two-dimensional energy followed by a long inertial range of an inverse two-dimensional energy cascade is to be put aside in this regime. Finally, we note that non-local energy transfers have also been noted in other anisotropic systems such as magnetohydrodynamic turbulence, where both non-local triads *and* non-local transfers characterize the exchange of energy between the velocity and magnetic field. Our findings suggest that modelling the dominant coupling between three-dimensional and two-dimensional vortices requires that the non-locality of the nonlinear interactions in the intermediate-*Ro* regime be accounted for. An

Forcing 1 (Cyl)				Forcing 2 (Disk)			
Ro	Ro_{2D}	F	Δt	Ro	Ro_{2D}	F	Δt
0.1	0.036	3.3×10^{-3}	2.6×10^{-3}	0.08	0.04	4.9×10^{-3}	2.6×10^{-3}
0.12	0.046	4.5×10^{-3}	2.6×10^{-3}	0.11	0.06	9.9×10^{-3}	2.6×10^{-3}
0.19	0.07	1.2×10^{-2}	2.6×10^{-3}	0.24	0.11	4.8×10^{-2}	2.6×10^{-3}
0.31	0.093	4.2×10^{-2}	2.6×10^{-3}	0.32	0.128	9.6×10^{-2}	2.6×10^{-3}
0.36	0.106	5.8×10^{-2}	2.6×10^{-3}	0.47	0.18	2.36×10^{-1}	2.6×10^{-3}
0.43	0.113	9.6×10^{-2}	2.6×10^{-3}	0.54	0.2	3.3×10^{-1}	2.6×10^{-3}
0.48	0.112	1.27×10^{-1}	2.2×10^{-3}	0.62	0.2	4.7×10^{-1}	2.6×10^{-3}
0.6	0.123	2.18×10^{-1}	1.5×10^{-3}	0.72	0.22	6.5×10^{-1}	2.6×10^{-3}
0.67	0.119	3.11×10^{-1}	1.5×10^{-3}	0.85	0.26	9.3×10^{-1}	1.9×10^{-3}
0.77	0.120	4.33×10^{-1}	1.5×10^{-3}	0.99	0.3	1.4	1.9×10^{-3}
0.94	0.117	7.22×10^{-1}	1.5×10^{-3}	1.15	0.2	1.87	1.9×10^{-3}
0.98	0.120	8.23×10^{-1}	1.5×10^{-3}	1.36	0.19	2.8	1.6×10^{-3}
1.5	0.166	3	1.5×10^{-3}	1.52	0.21	3.7	1.6×10^{-3}
2.3	0.242	9.7	1.5×10^{-3}	1.96	0.26	7.4	1.6×10^{-3}

TABLE 2. Ro, Ro_{2D}, forcing F, and time step Δt for each simulation of the set forced with the forcing F1 (left columns), and F2 (right columns). The hyperviscosity coefficient used for both sets is $\nu = 1.8 \times 10^{-24}$ and the rotation rate is $f = 2\Omega = 22.6 \text{ s}^{-1}$.

example of such modelling in classical two-dimensional turbulence can be found in e.g. Nazarenko & Laval (2000).

Appendix

In this appendix the parameters used for the series of simulations using F1 and F2 are given (table 2).

REFERENCES

ASSELIN, R. 1972 Frequency filter for time integrations. *Mon. Weath. Rev.* **100**, 487–490.

BABIN, A., MAHALOV, A. & NICOLAENKO, B. 1996 Global splitting, integrability and regularity of 3d euler and Navier–Stokes equations for uniformly rotating fluids. *Eur. J. Mech. (*B/*Fluids)* **15**, 291–300.

BABIN, A., MAHALOV, A. & NICOLAENKO, B. 2000 Global regularity of 3d rotating Navier–Stokes equations for resonant domains. *Appl. Maths Lett.* **13**, 51–57.

BARDINA, J., FERZIGER, J. H. & ROGALLO, R. S. 1985 Effect of rotation on isotropic turbulence: computation and modelling. *J. Fluid Mech.* **154**, 321–336.

BARTELLO, P., MÉTAIS, O. & LESIEUR, M. 1994 Coherent structures in rotating three-dimensional turbulence. *J. Fluid Mech.* **273**, 1–29.

BELLET, F., GODEFERD, F., SCOTT, J. & CAMBON, C. 2006 Wave-turbulence in rapidly rotating flows. *J. Fluid Mech.* **562**, 83–121.

BEWLEY, G. P., LATHROP, D. P., MAAS, L. R. M. & SCREENIVASAN, K. R. 2007 Inertial waves in rotating grid turbulence. *Phys. Fluids* **19**, 071701-1–071701-4.

BOUROUIBA, L. 2008*a* Discreteness and resolution effects in rapidly rotating turbulence. *Phys. Rev. E* **78**, 056309-1–056309-12.

BOUROUIBA, L. 2008*b* Model of truncated fast rotating flow at infinite Reynolds number. *Phys. Fluids* **20**, 075112-1–075112-14.

BOUROUIBA, L. & BARTELLO, P. 2007 The intermediate Rossby number range and 2d–3d transfers in rotating decaying homogeneous turbulence. *J. Fluid Mech.* **587**, 139–161.

BOYD, J. P. 1989 *Chebyshev & Fourier Spectral Methods*. Springer.

CAMBON, C. & SCOTT, J. F. 1999 Linear and nonlinear models of anisotropic turbulence. *Annu. Rev. Fluid Mech.* **31**, 1–53.

CANUTO, V. M. & DUBOVIKOV, M. S. 1997 Physical regimes and dimensional structure of rotating turbulence. *Phys. Rev. Lett.* **78**, 666–669.

CHEN, Q., CHEN, S., EYINK, G. L. & HOLM, D. D. 2005 Resonant interactions in rotating homogeneous three-dimensional turbulence. *J. Fluid Mech.* **542**, 139–164.

CHERTKOV, M., CONNAUGHTON, C., KOLOKOLOV, I. & LEBEDEV, V. 2007 Dynamics of energy condensation in two-dimensional turbulence. *Phys. Rev. Lett.* **99**, 084501-1–084501-4.

DOMARADSKI, J. A. 1988 Analysis of energy transfer in direct numerical simulations of isotropic turbulence. *Phys. Fluids* **31**, 2747–2749.

DOMARADZKI, J. A. & CARATI, D. 2007 An analysis of the energy transfer and the locality of nonlinear interactions in turbulence. *Phys. Fluids* **19** (8), 085112.

GREENSPAN, H. P. 1968 *The Theory of Rotating Fluid*. Cambridge University Press.

HIDE, R. & IBBERTSON, A. 1966 An experimental study of Taylor columns. *Icarus* **5**, 279–290.

HOPFINGER, E. J., BROWAND, K. F. & GAGNE, Y. 1982 Turbulence and waves in a rotating tank. *J. Fluid Mech.* **125**, 505–534.

HOSSAIN, M. 1994 Reduction in the dimensionality of turbulence due to strong rotation. *Phys. Fluids* **6**, 1077–1080.

IBBETSON, A. & TRITTON, D. J. 1975 Experiments on turbulence in a rotating fluid. *J. Fluid Mech.* **68**, 639–672.

JACQUIN, L., LEUCHTER, O., CAMBON, C. & MATHIEU, J. 1990 Homogeneous turbulence in the presence of rotation. *J. Fluid Mech.* **220**, 1–52.

KOLMOGOROV, A. N. 1941 The local structure of turbulence in incompressible viscous fluid for very large Reynolds number. *Dokl. Akad. Nauk SSSR* **30**, 301–305.

LESIEUR, M. 1997 *Turbulence in Fluids*, 3rd edn. Kluwer.

MCEWAN, A. D. 1976 Angular momentum diffusion and the initiation of cyclones. *Nature* **260**, 126–128.

MININNI, P. D., ALEXAKIS, A. & POUQUET, A. 2009 Scale interactions and scaling laws in rotating flows at moderate rossby numbers and large Reynolds numbers. *Phys. Fluids* **21** (1), 015108.

MORIZE, C. & MOISY, F. 2006 Energy decay of rotating turbulence with confinement effects. *Phys. Fluids* **18**, 065107-1–065107-9.

NAZARENKO, S. & LAVAL, J.-P. 2000 Non-local two-dimensional turbulence and batchelor's regime for passive scalars. *J. Fluid Mech.* **403**, 301–321.

PEDLOSKY, J. 1987 *Geophysical Fluid Dynamics*, 2nd edn. Springer.

SMITH, L. M. & WALEFFE, F. 1999 Transfer of energy to two-dimensional large scales in forced, rotating three-dimensional turbulence. *Phys. Fluids* **11**, 1608–1622.

STAPLEHURST, P. J., DAVIDSON, P. A. & DALZIEL, S. B. 2008 Structure formation in homogeneous freely decaying rotating turbulence. *J. Fluid Mech.* **598**, 81–105.

THIELE, M. & MÜLLER, W.-C. 2009 Structure and decay of rotating homogeneous turbulence. *J. Fluid Mech.* **637**, 425–442.

WALEFFE, F. 1993 Inertial transfers in the helical decomposition. *Phys. Fluids* **5**, 677–685.

WATANABE, T. I. T. & SHEPHERD, T. G. 2001 Infrared dynamics of decaying two-dimensional turbulence governed by the Charney–Hasegawa–Mima equation. *J. Phys. Soc. Japan* **70**, 376–386.

YEUNG, P. K. & ZHOU, Y. 1998 Numerical study of rotating turbulence with external forcing. *Phys. Fluids* **10**, 2895–2909.

ZHOU, Y. 1993*a* Degrees of locality of energy transfer in the inertial range. *Phys. Fluids* A **5** (5), 1092–1094.

ZHOU, Y. 1993*b* Interacting scales and energy transfer in isotropic turbulence. *Phys. Fluids* A **5**, 2511–2524.

ZHOU, Y. 1995 A phenomenological treatment of rotating turbulence. *Phys. Fluids* **7**, 2092–2094.